Title
Dynamical Bonding Driving Mixed Valency in a Metal Boride

Journal
Angewandte Chemie International Edition, 59(27)

ISSN
1433-7851

Authors
Robinson, Paul J
Munarriz, Julen
Valentine, Michael E
et al.

Publication Date
2020-06-26

DOI
10.1002/anie.202000945

Peer reviewed

Dynamical Bonding Driving Mixed Valency in a Metal Boride

Paul J. Robinson,[1,†] Michael E. Valentine,[2] Austin Granmoe,[2] Natalia Drichko,[2,*] Juan R. Chamorro,[2,3] Priscila F. Rosa,[4] Tyrel M. McQueen,[2,3,5,*] and Anastassia N. Alexandrova[1,6,*]

[1] Department of Chemistry and Biochemistry, University of California Los Angeles, Los Angeles, California 90095, USA
[2] Institute for Quantum Matter, Department of Physics and Astronomy, The Johns Hopkins University, Baltimore, Maryland 21218, USA
[3] Department of Chemistry, The Johns Hopkins University, Baltimore, Maryland 21218, USA
[4] Los Alamos National Laboratory, Los Alamos, NM 87545, USA
[5] Department of Materials Science and Engineering, The Johns Hopkins University, Baltimore, Maryland 21218, USA
[6] California NanoSystems Institute, Los Angeles, California 90095, USA

* drichko@jhu.edu, mcqueen@jhu.edu, ana@chem.ucla.edu

Classification: Physical Sciences, Chemistry
Keywords: Mixed Valency, Dynamical Bonding, Samarium Hexaboride, Chemical Bonding, Raman Spectroscopy

[†] Current Address: Department of Chemistry, Columbia University, New York, New York 10027, USA

Abstract

Samarium hexaboride is an anomaly, having many exotic and seemingly mutually incompatible properties. It was proposed to be a mixed-valent semiconductor, and later - a topological Kondo insulator, and yet has a Fermi surface despite being an insulator. We propose a new and unified understanding of SmB_6 centered on the hitherto unrecognized dynamical bonding effect: the coexistence of two Sm-B bonding modes within SmB_6, corresponding to different oxidation states of the Sm. The mixed valency arises in SmB_6 from thermal population of these distinct minima enabled by motion of B. Our model simultaneously explains the thermal valence fluctuations, appearance of magnetic Fermi surface, excess entropy at low temperatures, pressure-induced phase transitions, and related features in Raman spectra and their unexpected dependence on temperature and boron isotope.

Significance Statement

Samarium Hexaboride (SmB_6) has been attracting interest since its classification nearly 50 years ago. It possesses a plethora of puzzling and seemingly mutually-incompatible properties, from homogeneous Sm(II)/Sm(III) mixed valency, to pressure-induced phase transitions, unexpected Raman peaks, and unusual behavior of the specific heat at low temperature. We find that the Sm and B atoms in the lattice form in two distinct bonding minima controlling the mixed valency through their thermal populations, enabled by the motion of electron-carrying boron. This is a distinct new mechanism of mixed valency. The paradigm enables a unified understanding of many of the disparate properties of SmB_6, and a prediction of the Raman response to B isotope that we confirmed experimentally.

Samarium hexaboride (SmB_6) is a famously confusing solid, having attracted constant attention since its characterization (1). Nearly fifty years later, the ground state of SmB_6 remains unresolved (2,3). SmB_6 as a Kondo insulator is an intuitive thought: a three-band model predicts that the localized f-orbital peak at the Fermi level will hybridize with the d-orbitals and open a gap making an insulator. This would normally preclude the existence of a Fermi surface and thus remove any quantum oscillations, a signature of Landau quantization of a Fermi surface in a magnetic field. However, SmB_6 displays quantum oscillations (4-8). While a 2D Fermi surface can be a result of the presence of topological surface states (7), a 3D Fermi surface (9,10) is in contradiction with apparently insulating properties of the material. Many theories point to a topological type Kondo insulator allowing conduction only on the surface states, and some also point to composite particle excitons (11), and even call SmB_6 a Majorana Fermion sea (12,13). Other phenomena in SmB_6 are a resistivity plateau (14), and an anomalous peak in the specific heat (15), at T~100K.

The central enigmatic property of SmB_6 is its homogeneous mixed valency. The lattice of SmB_6 is cubic, but spectroscopic studies reveal two distinct oxidation states, Sm^{+2} and Sm^{+3} without an intermediate $Sm^{+2.5}$ state. In contrast to other mixed-valence compounds, SmB_6 does not show charge order. The ratio between the two valencies responds to *T* and *p* (16,17). The valency increases rapidly from around +2.5 at 0 K to a plateau at +2.6 above 100 K. This raises a chemical question: what type of mixed valency is the solid? The traditional Robin-Day scheme defines Types I-III mixed valency, corresponding to weak, medium, and strong couplings between two electronic states (e.g. $M^{2+}M^{3+}$ and $M^{3+}M^{2+}$), respectively (18). However, the T-dependence puts in question how much the mixed valency in SmB_6 conforms to these known schemes. For some rare-earth and actinide compounds, valence instabilities and transitions with *T*, *p*, and composition, are documented (19), and described mainly through band models, which consider valence transitions between a localized f-state and a delocalized band state (neither being precisely defined) (20). The energy of the localized states can rise in response to lattice compression, producing pressure effects. A seemingly disconnected theory for SmB_6 states that the ratio between Sm^{2+} and Sm^{3+} is held constant by the stiff, non-interacting boron network pressing against the hard sphere metal ions, while mixing Sm^{2+} and Sm^{3+} - cations of different radii - minimized the lattice energy (1). The major assumption underlying this description is the lack of electronic Sm-B interactions, whereas in other borides M-B interactions were found to be prominent (21-23), and sensitive to mechanical stress (24,25). Hence, there has never been a satisfying microscopic theory explaining the origin of the mixed valency in SmB_6.

In this paper, we present a unifying dynamic bonding model of SmB_6, which readily explains its mixed valency, valence fluctuations and changes with *T* and *p*, and predicts many seemingly disparate properties such as peak in heat capacity, and Raman scattering spectra associated with valency changes. We will build the solid from the ground up, starting with molecular clusters that reveal the key bonding elements present also in the solid, as suggested by Hoffmann, Pauling, and several followers (26-31). Then, we reconstruct the chemically informed model of the full SmB_6 solid. The approach is necessitated by the intractably complex electronic structure of SmB_6: strongly multireference, and relativistic (for Sm, the spin-orbit (SO) splitting between the J=5/2 and J=7/2 states is comparable to the crystal field splitting) (32). These effects inevitably present a problem for DFT, but remain firmly out of reach for even

the most sophisticated ab initio methods. The key to our model is the unique and dynamic bonding interactions between Sm and B (33).

First, we examine the structural motifs present in SmB_6 and identify the key bonding interactions. A minimal cluster needn't be stoichiometrically identical to the solid; in fact the SmB_6^- cluster has been studied theoretically and spectroscopically, and showed no resemblance with the material (33). SmB_6 has a cubic unit cell with a B_6 octahedron in the center; however, the B-B distance between cells is shorter than within the octahedron, suggestive of B_2 dimers. A plane-wave DFT calculation on this geometry reveals that the electrons are localized in-between the cells much more than in the octahedron (Fig. S1). Thus, considering SmB_6 as built of Sm and B_2 units brings us to SmB_2^+ as a minimal cluster model. The positive charge mitigates the undercoordinated environment of a gas phase cluster compared to the crystal. This cluster is small enough to explicitly calculate many-body and relativistic effects, and to qualitatively inform about the bonding motifs possible in the solid.

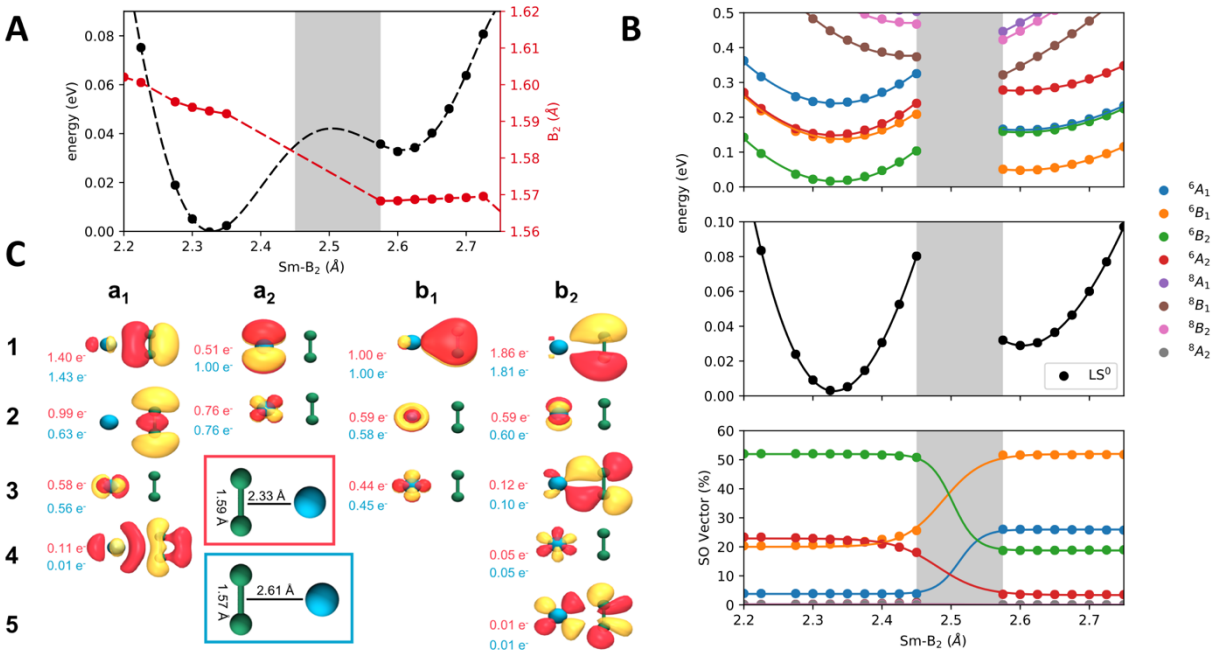

Figure 1: SmB_2^+ minimal cluster model. A: Ground state energy (black) at the lowest energy B_2 bond length (red) across the range of Sm-B_2 bond lengths. B: Scan across Sm-B_2 bond lengths with B_2 fixed at 1.57 Å. Top: 8-state CASSCF(14,9) scan. The energy calculations are well behaved except for in the greyed crossover between the areas of $^6B_1$ and $^6B_2$ dominance. Middle: the spin-orbit ground state (LS^0), and Bottom: its composition. Even in the well-behaved areas of the potential energy surface the ground state is strongly SO-coupled and contains nearly 50% states other than the leading term. C: The active space orbitals, and the occupations for the two minima (geometries of the minima are shown in the insets: green –B_2 dimer at the center of the face in the cubic lattice, blue – Sm in the vertex of the cube, interacting with B_2). The oxidation state of Sm switches between the two minima. Localized electrons from a lone pair 5d orbital ($1a_2$) shift to the $\sigma(p_z)$ bonding states of B_2 ($2a_1$).

Unexpectedly, the ground state potential energy surface of SmB_2^+ has two nearly degenerate bonding minima, one with the B-B bond length of 1.59 Å and the Sm-B_2 distance of 2.33 Å, and the other with the B-B bond length of 1.57 Å and the Sm-B_2 distance of 2.61 Å (Figure 1A and C). The energy difference between the minima is only 33 meV, suggestive of

easy interconversion on short timescales. The two minima are predominantly $^6B_1$ and $^6B_2$, though both have large additional contributions from other states (Figure 1B). The electronic transition between the minima is achieved by nuclear motion, and enabled by strong nonadiabatic coupling, including spin-orbit (SO). Most of the orbitals in the active space remain constantly occupied during the transition and in the minima (Figure 1C), and many correspond to Sm-B bonds, directly contrasting the long-held presumption of boron's innocence. There is one crucial bonding difference between the minima: a significant shift of electrons from $1a_2$ to $2a_1$, corresponding to a charge transfer from a d_{xy} orbital on Sm to an isolated $\sigma(p_z)$ bond on B_2 (the LUMO of the B_2 molecule), consistent with the Sm-d form factor in the neutron scattering. The transfer is accompanied by the energy-reordering of $1a_2$ to $2a_1$. Whichever of these two orbitals is occupied will determine the oxidation state of the Sm. Therefore, the small stretch and displacement of the B_2 causes the change of the electronic configuration and charge transfer. The oxidation state of Sm is thus controlled by motion of boron. In the SmB_6 solid, this motion is achieved through vibrations.

Explicitly computing the two states and the vibronically-enabled transition between them in the solid is not feasible, but we gather significant evidence that the two minima are present. DFT provides a qualitative agreement: upon an artificial deformation of the lattice where B_2 is displaced toward one of the Sm ions by 20 % of the equilibrium Sm-B_2 distance, the B_2 $\sigma(p_z)$ state moves from the valence to the virtual manifold, as predicted by our cluster model (Fig. S2). The average valence measured by Mössbauer is static over changes in *T*, whereas X-ray absorption shows the increase of valence with *T* (16). Our model resolves this discrepancy by predicting a constant ratio of f-shell occupations (which Mössbauer measures), and a variable d-orbital occupation (not seen by the Mössbauer). Indeed, our minimal cluster model shows the Sm(II) $\rightarrow$ Sm(III) + e^- transition as $4f^55d^16s^0 \rightarrow 4f^55d^06s^0 + e^-$, enabled by boron motion. Hence, we have strong initial indications that the solid SmB_6 also has two distinct bonded states available to every B_2 with every Sm in the face of the cube. Based on this "two-state" model, we now construct the model of the full solid.

For the face of the cubic lattice, consisting of four Sm atoms and one B_2, we thus predict a 5-well system (Figure 2A), with four energy-degenerate wells where one out of four Sm ions is in the +2 oxidation state ('reduced') and B_2 is stretched and displaced toward this Sm, and a non-degenerate central well where the B-B distance is compressed, B_2 holds an extra electron in the bonding $\sigma(p_z)$-orbital, and all Sm ions are in the +3 oxidation state ('oxidized'). The relative energies and geometries of these minima in the solid likely differ from those in the cluster. The energy-displacement between the minima presents three distinct possibilities for the character of the mixed valent system (Figure 2A right). First, the oxidized state can be lower in energy than the reduced states, and this case results in a symmetric oxidized ground state and thermal population of the reduced states. Second, the oxidized state can be higher in energy than the reduced states but lower than the barrier to interconversion between the states. This system would undergo transitions between the reduced minima with different Sm ions in the +2 state, and the ground state would be symmetry-broken. Finally, the oxidized minimum can be higher in energy than the interconversion barrier between the reduced wells. The mixed valency in this case will not be affected by the oxidized state, and it falls into one of the three Robin-Day schemes.

The free parameter in the model is the energetic splitting ϵ between the reduced and oxidized minima. Instead of using ϵ from the cluster model, or calculating it for the solid *ab inito*, we find it from fitting to experiment. Given that only one Sm in every face of the cube can interact with B_2, we can state that, when B_2 interacts with the Sm, the average oxidation state of Sm in the solid will be +2.5, while when B_2 is non-interacting, the average oxidation state of Sm will be in the +3. The dimensionality of the problem is thus reduced to a set of cluster states embedded in the solid. Using x-ray absorption average valency data as a function of T,[16] we performed a least-squares fit to the functional form shown in Figure 2B, and found the energy splitting, ϵ, in the solid to be 5.2 meV. The reduced minima appear lower in energy than the oxidized minimum. The fitted degeneracy of the reduced states, d, is 4.05 as expected.

The model yields the following description of mixed valence in SmB_6: Below 10 K, the solid is almost entirely in the ground state with an average valency of +2.5. The B_2 dimers hold no extra electrons, remain stretched, and displaced toward one of the Sm, creating structural disorder in the boron sublattice. Between ca. 10 K and 100 K, the thermal excitations begin allowing B_2 to exit the reduced minima, now holding an extra electron, and leaving Sm in the +3 oxidation state. Hence, valency increases rapidly until beginning to taper off towards an asymptotic average of +2.6.

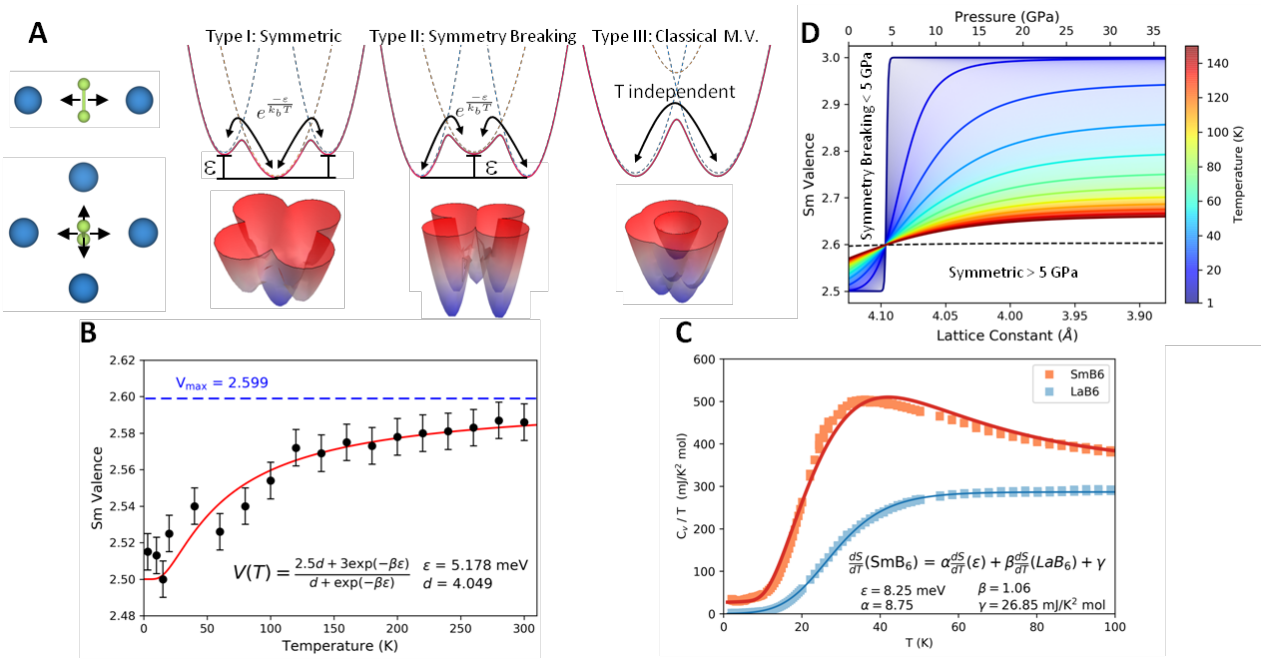

Figure 2: Model of SmB_6 solid based on the dually accessible bonding states. A: top: one-dimensional three-well model displaying the three classes of mixed valency that can occur with a variable central well height and their thermodynamic populations. Bottom: two-dimensional analogues of the displacements and well types as they would be seen in the solid B: Least squares two-level thermodynamic fit to the x-ray absorption mixed valency data. The two free parameters d and ε are the degeneracy of the side states and the energy splitting respectively. C: Fitting of the excess entropy to the toy model. The modes from the rest of the solid are accounted for by scaling the profile of LaB_6 and adding the additional peak on top. D: Demonstration of a transition between mixed valency types induced by pressure calculated from x-ray data over different pressures. Note the discontinuous jump of average Sm valence from +2.5 to +3 at 5 GPa signals a phase transition from symmetry broken to symmetric mixed valency. Using the parameters calculated in section B.

Vibronic coupling thus appears to be the key to mixed valency in SmB_6. Evidence of the electron-phonon interactions between the B-B stretch in the B_2 dimers and the electrons in Sm comes from Raman vibrational spectroscopy.

Guided by the model, we tested the dependence of Raman spectra of SmB_6 on the ^{10}B / ^{11}B isotope substitution. The spectra show a broad continuum of excitations extending to frequencies above 200 meV, with narrow features of phonons superimposed on it at frequencies between approximately 80 and 175 meV (Figure 3A). The continuum is assigned to the excitations between the bands of Sm, which develop a hybridization gap at low temperatures (34). The phonons are Raman active boron-motion related phonons, which shift in frequency upon isotope substitution from ^{10}B to ^{11}B as expected according to the regular dependence of frequency on mass as $\omega \sim \sqrt{\frac{m(^{11}B)}{m(^{10}B)}}$. The line width of the phonons that do not interact with electrons, Γ, is defined by a natural width Γ_N for pure isotopes, and $\Gamma_N + \Gamma_D$ for partial isotope substitution. Γ_D depends on disorder (Figure 3B), as demonstrated by the E_g and T_{1g} phonons, which show an increased width for samples with mixed isotope content. The highest frequency A_{1g} phonon is an exception from this rule. It shows an asymmetric so-called Fano shape [see SI], typical for phonons coupled to an underlying continuum of interband excitations of electrons of Sm (35). The constant width Γ of A_{1g} for all levels of isotope substitution suggests that it is defined by the electron-phonon coupling. This strong electron-phonon interaction is in agreement with our model, where an in-phase stretch of the B-B bonds in the B_2 dimers (Figure 3D) is associated with Sm-B_2 electronic interactions responsible for the lowering of the oxidation state of the Sm.

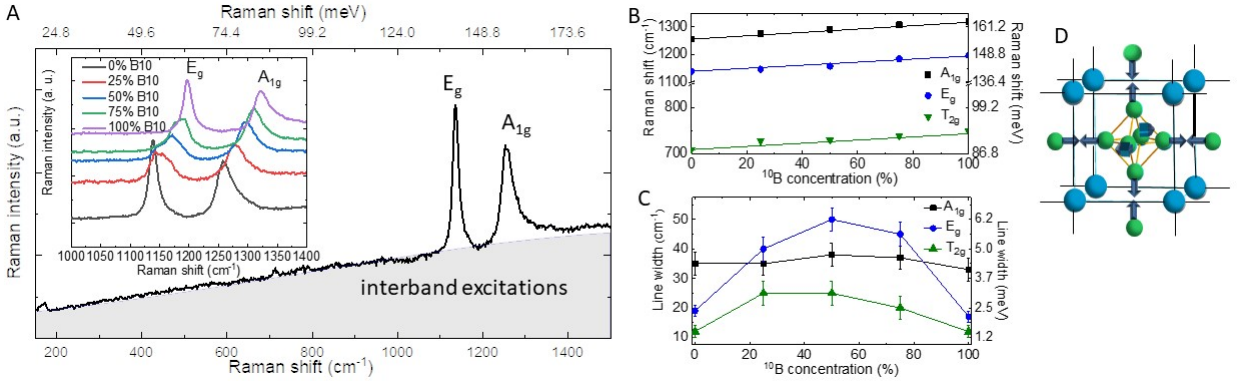

Figure 3. Electron-phonon coupling revealed by boron-motion-related phonons of SmB_6 **A:** Raman scattering spectrum of $Sm^{11}B_6$ in A_{1g}+E_g symmetry. Phonons are superimposed on the continuum of interband excitations. A_{1g} phonon shows an asymmetric shape due to the interactions with the interband excitations. Inset shows phonon spectra of isotope substituted SmB_6 for A_{1g}+Eg symmetry, shifted along Y axis for clarity; note the linear increase of frequency upon changing from ^{11}B to ^{10}B (plotted in **B**), and an increase of the width of the E_g and T_{2g} phonons for partially substituted samples (plotted in **C**). **D:** The A_{1g} phonon of SmB_6 following calculations presented in Ref. (36). Note that it involves in-phase stretching vibrations of all B-B pairs.

Raman spectra of SmB_6 also show a number of features in the energy range of interest identified by our model (Figure 4A): We observe two overlapping features at ca. 22 meV

marked as F1 in Figure 4, one of which is a sharp phonon-like (red circle), and the other is much broader (black square). Lattice optical T_{1u} phonons involving movement of both boron and Sm are a good candidate for an excitation observed in this frequency range. (36,37) This assignment is confirmed by the boron isotope-dependent frequency shift of the sharp feature. Indeed, while low frequency of around 20 meV where the phonon is observed is defined by the large mass of Sm atom, the feature shifts by ca. 0.17 meV towards the higher frequency upon replacement of ^{11}B with ^{10}B (Figure 4A). This phonon modulates the distance between B_2 and Sm atoms, which within our model leads to valence fluctuations. In the absence of electron-phonon coupling T_{1u} phonons are forbidden in Raman scattering of SmB_6. Valence fluctuations lead to relaxing of the selection rules, and to an appearance of an additional broad excitation which is associated with a local lattice deformation and a transfer of an electron from Sm to B_2.

While our model for the first time gives a detailed microscopic description of the valence fluctuations phenomena in SmB_6, the general picture resonates with the theory of exiton-polaron excitations developed in Ref. [37-38]. The A_{1g} symmetry of the features at about 20 meV (Figure 4D) is in agreement with the suggested symmetry of the valence fluctuations.(37,38) Below 50 K the linewidth of the narrow feature of the T_{1u} phonon starts to decrease, while the feature shifts to higher frequencies (Figure 4C), evidencing that the system descends more deeply in the reduced minima, away from the unharmonic regime and strongest vibronic coupling. The behavior follows the suggestion of our model, where the system freezes at the bottom of the reduced minima at low *T*, leading to the +2.5 average valency of Sm. On the other hand, the mixed exiton-polaron excitation shows lower bandwidth in the higher-temperature regime, when the exciton-polaron is in a hopping regime and is suggested to have longer life-time in each site (38).

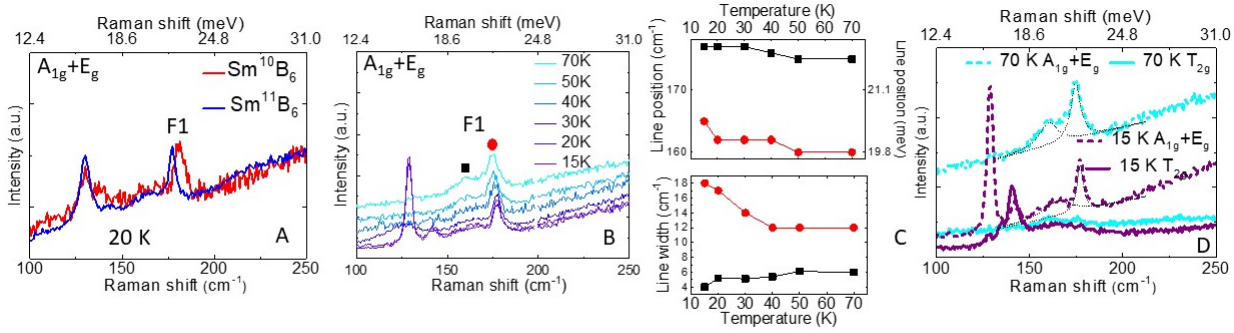

Figure 4. Raman spectra in the range between 12.4 and 30 meV where valence fluctuations-related feature (F1) is observed. **A:** Spectra of SmB_6 with fully pure ^{10}B and ^{11}B isotopes in $A_{1g}+E_g$ scattering channel at 20 K. Note that isotope shift is observed for the feature related to optical phonon at about 22 meV, while position of spin exciton at 16 meV does not change. **B-C:** SmB_6 (natural isotope mix) $A_{1g}+E_g$ scattering channel, temperature dependence of the spectra and lines positions and width for features related to valence fluctuations. Note that the broad exiton-polaron excitation broadens considerably on cooing below 40 K, while the narrow phonon-related feature gets somewhat narrower. **D:** Comparison of $A_{1g}+E_g$ and T_{1g} symmetry spectra. Fitting curves for the lattice phonon and exciton-polaron excitations are shown for 15 and 70 K with black dashed curves. Note that the features related to valence fluctuations are observed only in A_{1g}.

Hence, both theory and spectroscopy point at rich vibronic behavior of SmB_6. On the basis of this understanding, we now address the question of why SmB_6 has an anomalous peak

in $\left.\frac{dS}{dT}\right|_V$ at around 20 K (15). Normally, one would expect $\left.\frac{dS}{dT}\right|_V$ to decrease with *T*, as the phonons gradually freeze out. The additional peak points towards an unexplained energy scale in SmB_6. From our model, we derive the expression for the entropy and calculate its maximum at 19.6 K—in agreement with experiment (derivations presented in the SI). We interpret the anomalous peak in entropy as follows: at low *T*, vibrational entropy builds up from the motion of the B_2 units within the reduced minima; as *T* rises, B_2 units unfreeze from the reduced minima and gain a new vibrational freedom, the lattice changes symmetry, and the vibrational partition function qualitatively changes its nature. Here we obtain a second, independent, method of finding the energy splitting, ϵ, (Figure 2C). Specifically, we find quantitative agreement with the experiment for the excess entropy when ϵ = 8.25 meV, similar to the first estimation, with the difference likely arising from the simplicity of the model.

Average valency in SmB_6 also responds to pressure. With increasing *p*, it increases past what would be allowed by thermal population, e.g. at 35 GPa the average valency approaches +3 (17). Curiously, the average valency never reaches +3 nor is it affected by a phase transition from a non-magnetic to magnetic material at 5 GPa. Indeed, as Butch et all point out (17), this result challenges prior explanations of intermediate valence in SmB_6 that do not predict the mixed valency remaining stable at high pressure. Microscopically, pressure shrinks the unit cell and thus crowds the Sm closer to the B_2 units. From the cluster model, we see that the oxidized Sm-B_2 minimum is more easily compressed than the reduced minimum, with the force constants of 6.4 eV $Å^{-2}$ and 14.2 eV $Å^{-2}$, respectively. Hence, at rising *p*, the reduced minima rise in energy, eventually going above the oxidized minimum, which becomes the new ground state, leading to a phase transition.

To test this hypothesis, we calculate the energy splitting ϵ for each experimentally tested *p*, and found that it decreases with added *p*. At 5 GPa the material undergoes a first order phase transition from the system where the central oxidized state mediates the transitions between the reduced states through boron motion, to the system where the oxidized state is lower in energy and dominates, as evidenced by a discontinuity in the average valency (Figure 2D). This lends an explanation to the observed transition from non-magnetic to magnetic solid at that pressure: the conducting and magnetic phase corresponds to the oxidized state, where boron holds an extra electron and thus a spin. This also provides an answer for why below 5 GPa, the solid has a ground state average valency of +2.5 while above 5 GPa the solid has a ground state average valency near +3. However, for any $T > 0$ K, adding *p* will never cause the average valency to reach +3, due to thermal fluctuations and transient visits of boron closer to Sm. It's worth noting that at $k_bT \gg \epsilon$ the phase transition is indiscernible.

Finally, we consider the outstanding problem of the quantum oscillations in SmB_6. Both 2D and 3D Fermi surfaces were reported for this insulating solid, although these conclusions are model-dependent and based on very similar data (38,39). Currently, the origin of quantum oscillations is understood as composite particles with zero overall charge and a non-zero spin. From our model, a potential physical origin of this many-body effect is as follows: Every Sm ion is in an electron-exchange relationship with one B_2 (we showed in a cluster model that every Sm can sustain the tighter bonded state with only one B_2 at a time). The full stoichiometric unit is required, however, for the charge neutrality. The B_2 dimer is too heavy to act as a large

conduction particle, hence the low charge mobility, but it nonetheless possesses a spin. In a magnetic field, it will experience a Lorentz force and its motion will become Landau quantized, resulting in the appearance of a magnetic Fermi surface. Each B_2 is confined to a single plane, and the Sm-B_2 motifs form a 3-D crystal, explaining the ambiguous magnetic Fermi surface.

In summary, we present a new paradigm for SmB_6 in which strong vibronic effects allow the coexistence of five distinct bonding possibilities for each B_2 unit connecting the neighboring unit cells. Through this new model we discovered a new class of mixed valency, distinct from the Robin-Day scheme; rather than being dependent on couplings of two reduced states, the mixed valency results from the population of a third, central, oxidized state. The existence of the extra states in the material, and the vibronic coupling between them, enabled by the boron motion, creates an additional, lower energy scale to the solid, accounting for excess entropy and an unexplained phase transition. Hand in hand, this model also suggests that the solid has hidden aperiodicity within it; namely, the B_2 units are disordered within the cubic Sm lattice at low *T*. This realization naturally leads to an explanation of why symmetry forbidden peaks persistently appear in Raman spectra of SmB_6. We also propose these cluster states to be the physical manifestations of theorized composite particles responsible for the observed magnetic Fermi surface.

Acknowledgements

A.N.A. acknowledges the support of the NSF CAREER Award (CHE-1351968). P.J.R. acknowledges support from the NSF Graduate Research Fellowship under Grant No. (DGE-1644869), and the UCLA Undergraduate Research Center—Sciences. Work at the Institute for Quantum Matter, an Energy Frontier Research Center, was funded by the U.S. Department of Energy, Office of Science, Office of Basic Energy Sciences, under Award DE-SC0019331.

References

1. Nickerson JC, White RM, Lee KN, Bachmann R, Geballe TH, Hull GW, Jr (1971) Physical properties of SmB_6. *Phys. Rev. B* 3:2030.

2. Cooley JC, Aronson MC, Fisk Z, Canfield PC (1995) SmB_6: Kondo insulator or exotic metal? *Phys. Rev. Lett.* 74:629.

3. Martin RM, Allen JW (1979) Theory of mixed valence: metals or small gap insulators. *J. Appl. Phys.* 50:7561-7566.

4. Li G, Xiang Z, Yu F, Asaba T, Lawson B, Cai P, Tinsman C, Berkley A, Wolgast S, Eo YS, Kim DJ (2014) Two-dimensional Fermi surfaces in Kondo insulator SmB_6. *Science* 346:1208-1212.

5. Jiang J, Li S, Zhang T, Sun Z, Chen F, R. Ye ZR, Xu M, Ge QQ, Tan SY, Niu XH, Xia M (2013) Observation of possible topological in-gap surface states in the Kondo insulator SmB_6 by photoemission. *Nat. Commun.* 4:3010.

6. Stern A, Dzero M, Galitski VM, Fisk Z, Xia J (2017) Surface-dominated conduction up to 240 K in the Kondo insulator SmB6 under strain. *Nat. Mater.* 16:708.

7. Kim DJ, Xia J, Fisk Z (2014) Topological surface state in the Kondo insulator samarium hexaboride. *Nat. Mater.* 13:466.

8. Park WK, Sun L, Noddings A, Kim DJ, Fisk Z, Greene LH (2016) Topological surface states interacting with bulk excitations in the Kondo insulator SmB_6 revealed via planar tunneling spectroscopy. *Proc. Natl. Acad. Sci. U.S.A.* 113:6599-6604.

9. Tan BS, Hsu YT, Zeng B, Hatnean MC, Harrison N, Zhu Z, Hartstein M, Kiourlappou M, Srivastava A, Johannes MS, Murphy TP (2015) Unconventional Fermi surface in an insulating state. *Science* 349:287-290.

10. Hartstein M, Toews WH, Hsu YT, Zeng B, Chen X, Hatnean MC, Zhang QR, Nakamura S, Padgett AS, Rodway-Gant G, Berk J (2018) Fermi surface in the absence of a Fermi liquid in the Kondo insulator SmB_6. *Nat. Phys.* 14:166–172.

11. Knolle J, Cooper NR (2017) Excitons in topological Kondo insulators: theory of thermodynamic and transport anomalies in SmB_6. *Phys. Rev. Lett.* 118:096604.
12. Baskaran G (2015) Majorana Fermi Sea in Insulating SmB_6: A proposal and a Theory of Quantum Oscillations in Kondo Insulators. arXiv:1507.03477v1. Preprint, posted July 13, 2015.
13. Erten O, Chang PY, Coleman P, Tsvelik AM (2017) Skyrme insulators: insulators at the brink of superconductivity. *Phys. Rev. Lett.* 119:057603.
14. Dzero M, Jing X, Victor G, Piers C (2016) Topological kondo insulators. *Annu. Rev. Condens. Matter Phys* 7:249-280.
15. Phelan WA, Koohpayeh SM, Cottingham P, Freeland JW, Leiner JC, Broholm CL, McQueen TM (2014) Correlation between bulk thermodynamic measurements and the low-temperature-resistance plateau in SmB_6. *Phys. Rev. X* 4:031012.
16. Mizumaki M, Tsutsui S, Iga F (2009) Temperature dependence of Sm valence in SmB_6 studied by X-ray absorption spectroscopy. *J. Phys. Conf. Ser.* 176:012034.
17. Butch NP, Paglione J, Chow P, Xiao Y, Marianetti CA, Booth CH, Jeffries JR (2016) Pressure-resistant intermediate valence in the Kondo insulator SmB_6. *Phys. Rev. Lett.* 116:156401.
18. Parthey M, Kaupp M (2014) Quantum-chemical insights into mixed-valence systems: within and beyond the Robin–Day scheme. *Chem. Soc. Rev.* 43:5067-5088.
19. Robinson JM (1979) Valence transitions and intermediate valence states in rare earth and actinide materials. *Phys. Rep.* 51:1-62.
20. Ramirez R, Falicov LM, Kimball JC (1970) Metal-insulator transitions: A simple theoretical model. *Phys. Rev. B* 2:3383.
21. Levine JB, Tolbert SH, Kaner RB (2009) Advancements in the search for superhard ultra-incompressible metal borides. *Adv Funct Mater.* 19:3519-3533.
22. Gilman JJ, Cumberland RW, Kaner RB (2006) Design of hard crystals *IJRMHM* 24:1-5.
23. Brazhkin VV, Lyapin AG, Hemley RJ (2002) Harder than diamond: dreams and reality. *Philos. Mag. A* 82:231-253.
24. Robinson PJ, Liu G, Ciborowski S, Martinez-Martinez C, Chamorro JR, Zhang X, McQueen TM, Bowen KH, Alexandrova AN (2017) Mystery of three borides: differential metal–boron bonding governing superhard structures. *Chem. Mater.* 29:9892-9896.
25. Lei J, Yeung MT, Robinson PJ, Mohammadi R, Turner CL, Yan J, Kavner A, Alexandrova AN, Kaner RB, Tolbert SH (2018) Understanding how bonding controls strength anisotropy in hard materials by comparing the high-pressure behavior of orthorhombic and tetragonal tungsten monoboride. *J. Phys. Chem. C* 122:5647-5656.
26. Pauling L (1948) The Metallic State. *Nature* 161:1019-1020.
27. Pauling L (1949) A resonating-valence-bond theory of metals and intermetallic compounds. *Proc. R. Soc. Lond. A* 196:343-362.
28. Hoffmann R (1987) How Chemistry and Physics Meet in the Solid State. *Angew. Chem. Int. Ed.* 26:846–878.
29. Burdett JK (1997) *Chemical Bonding in Solids* (Wiley).
30. Cox PA (1987) *The Electronic Structure and Chemistry of Solids* (Clarendon Press).
31. Canadell E, Doublet M-L, lung C (2012) *Orbital Approach to Electronic Structure of Solids* (Oxford University Press).
32. Jiao L, Rößler S, Kim DJ, Tjeng LH, Fisk Z, Steglich F, Wirth S (2016) Additional energy scale in SmB_6 at low-temperature. *Nat. Commun.* 7:13762.
33. Robinson PJ, Zhang X, McQueen TM, Bowen KH, Alexandrova AN (2017) SmB_6–cluster anion: covalency involving f orbitals. *J. Phys. Chem. A.* 121:1849-1854.
34. Valentine ME, Koohpayeh S, Phelan WA, McQueen TM, Rosa PF, Fisk Z, Drichko N (2016) Breakdown of the Kondo insulating state in SmB_6 by introducing Sm vacancies. *Phys. Rev. B.* 94:075102.
35. Fano U (1961) Effects of configuration interaction on intensities and phase shifts. *Phys. Rev.* 124:1866.
36. Ogita N, Nagai S, Okamoto N, Udagawa M, Iga F, Sera M, Akimitsu J, Kunii S (2003) Raman scattering investigation of RB_6 (R= Ca, La, Ce, Pr, Sm, Gd, Dy, and Yb). *Phys. Rev. B* 68:224305.
37. Alekseev PA (2015) High borides: determining the features and details of lattice dynamics from neutron spectroscopy. *Physics-Uspekhi* 58:330-344.

38. Erten O, Ghaemi P, Coleman P (2016) Kondo breakdown and quantum oscillations in SmB_6. *Phys. Rev. Lett.* 116:046403.
39. Hartstein M, Toews WH, Hsu YT, Zeng B, Chen X, Hatnean MC, Zhang QR, Nakamura S, Padgett AS, Rodway-Gant G, Berk J (2018) Fermi surface in the absence of a Fermi liquid in the Kondo insulator SmB_6. *Nat. Phys.* 14:166-172.

Supplementary Information:
Dynamical Bonding Driving Mixed Valency in a Metal Boride

Paul J. Robinson,[1,†] Michael E. Valentine,[2] Austin Granmoe,[2] Natalia Drichko,[2,*] Juan R. Chamorro,[2,3] Priscila F. Rosa[4] Tyrel M. McQueen,[2,3,5,*] and Anastassia N. Alexandrova[1,6,*]

[1] Department of Chemistry and Biochemistry, University of California Los Angeles, Los Angeles, California 90095, USA
[2] Institute for Quantum Matter, Department of Physics and Astronomy, The Johns Hopkins University, Baltimore, Maryland 21218, USA
[3] Department of Chemistry, The Johns Hopkins University, Baltimore, Maryland 21218, USA
[4] Los Alamos National Laboratory, Los Alamos, NM 87545, USA
[5] Department of Materials Science and Engineering, The Johns Hopkins University, Baltimore, Maryland 21218, USA
[6] California NanoSystems Institute, Los Angeles, California 90095, USA

*drichko@jhu.edu, mcqueen@jhu.edu, ana@chem.ucla.edu

[†] Current Address: Department of Chemistry, Columbia University, New York, New York 10027, USA

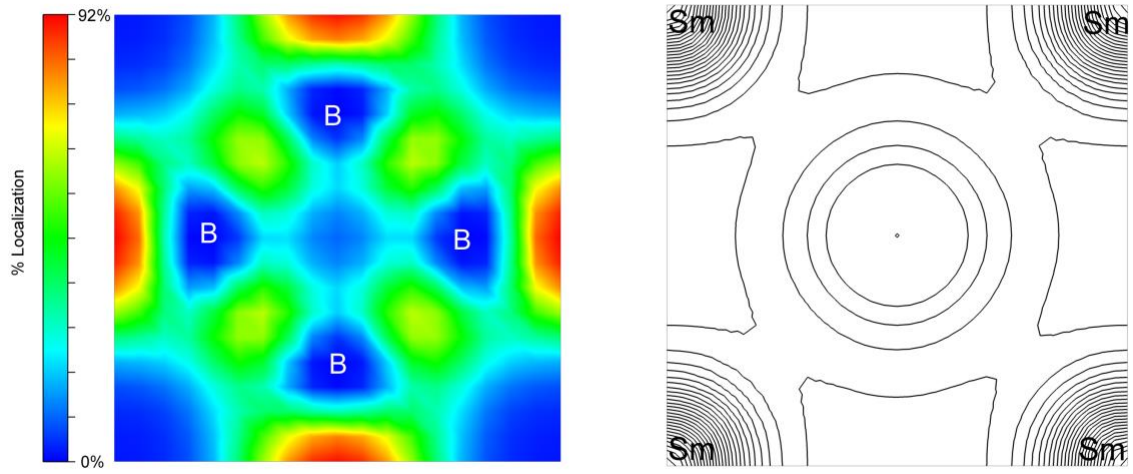

Figure S1: Left: The Electron Localization Function (ELF) of a crude DFT+U calculation. The electrons are significantly more localized between unit cells in the B_2 units than in the octahedron. Right: The charge density of the same calculation demonstrating a potential bonding interaction between a B_2 and the Sm.

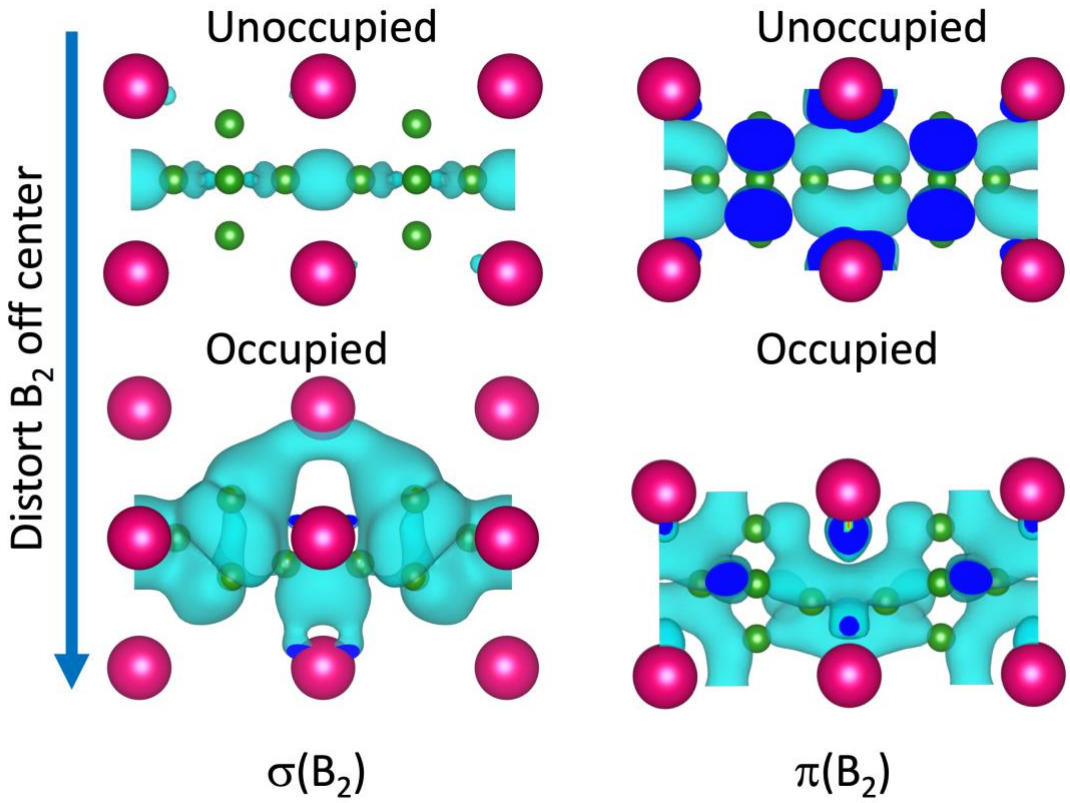

Figure S2: Artificial deformation displacing B_2 toward one of the Sm ions by 20 % of the equilibrium Sm-B_2 distance. At the gamma point the B_2 $\sigma(p_z)$ state goes from virtual to valence in agreement with our cluster model.

Computational Methods:

All molecular calculations were performed with Molpro.[1] For Sm the cc-pvDz-DK3[2] basis was used and for B the cc-pvDz[3] basis was used. We selected the sixth-order Douglass-Kroll-Hess Hamiltonian[4] to account for significant scalar relativistic effects beyond the second order present in Sm systems. Motivation for our choices of basis set and order of scalar relativistic correction can be found in a previous study of the SmB_6^- cluster. (Ref 33, main text)
The energy surface of SmB_2^+ was modeled with a 8-state CASSCF(14o,9e)+DKH6 with the lowest energy octet and sextet A_1 A_2 B_1 and B_2 states. The spin-orbit ground state was then obtained from coupling all eight of these states. The optimized B_2 length was computed at each Sm-B_2 bond length by fitting a quadratic function to several points sampled by the minimum. The $B_2SmB_2^{2+}$ cluster was modeled in several different charges and states with a CASSCF(19o,12e)+DKH6. Because of the high symmetry and many accessible electronic configurations, we found it necessary even for our qualitative understanding to use an active space of this size.

It is important to confirm that our selected three atom cluster doesn't ignore important interactions in the solid. Namely, does the addition of more than one B_2 unit change the bonding. To check this, we model the $[B_2\text{-}Sm\text{-}B_2]^{+2}$ cluster's $^9A_2$ state. Optimized, we see that Sm bonds covalently with one of the B_2 units and is nearly non-interacting with the other as evidenced by the Sm-B_2 bond lengths of 2.38 Å and 3.09 Å respectively. Considering that in the solid the Sm is always found in at least a +2 state we can understand this result. A Sm coordinated to 3 B_2 units (SmB_6) will have donated electrons to two of its three adjacent B_2 units making them non-interacting. Knowing this, we return to our smaller, more approachable, model to understand the intricacies of Sm-B_2 bonding while remaining confident that only one B_2 interacts with a single Sm at a time.

Analytic Model

Considering the bulk solid as an ensemble of small two state clusters, we incorporate the energy difference between these states as a thermodynamic parameter. Now, we write a temperature dependent expression for the average Sm valence where the valence depends on which level the system is in.

$$\mathrm{V}(T) = \frac{2.5d + 3\exp(-\beta\epsilon)}{d + \exp(-\beta\epsilon)}$$

We use the standard $\beta = (\mathrm{T}\ k_b)^{-1}$. We set d to the degeneracy of the lower level and allow it to vary in our expression rather than setting it to four like in figure 2A. This serves a validating purpose; it's a parameter that we know should be very near four, so if experimental valency data is fit to this function it should indeed be near four.

Considering our dual bonding minima, it is straightforward to use calculate the specific heat for such a two-level system. As such, the $C_v\ T^{-1}$ component from the cluster state is written as:

$$\frac{dS}{dT} = \frac{1}{T^3}\frac{\epsilon^2 d\exp\left(\frac{\epsilon}{k_b T}\right)}{k_b\left(1 + d\exp\left(\frac{\epsilon}{k_b T}\right)\right)^2}$$

In order to achieve quantitative agreement with the experimental data, it is important to remove the contribution from all of the other motions in the solid. Using the C_vT^{-1} profile of LaB_6 as a base, we can isolate the contributions of our cluster from the rest of the solid. Scaling the above equation for $C_v\ T^{-1}$ by some degeneracy (α), adding the mass-scaled (β) specific heat of LaB_6, and adding a zero-temperature constant (γ) generates an equation that we can fit to experimental data.

$$\frac{dS}{dT}(\mathrm{SmB_6}) = \alpha\frac{dS}{dT}(\epsilon) + \beta\frac{dS}{dT}(\mathrm{LaB_6}) + \gamma$$

As seen in main text Figure 4D, the optimized parameters have clear physical meanings. α is the degeneracy of the total cluster system's ground state surface, β is roughly the scaling of masses between Sm and La.

To establish a connection between epsilon and pressure we rewrite epsilon as a function of valence. Working from our expression for the average valence, we write a new expression for the change in $\varepsilon\ k_b^{-1}T^{-1}$.

$$\frac{\epsilon}{k_bT} = -\ln\left(\frac{Vd - d(2.5)}{3 - V}\right)$$

Discussion on the relationship of the SmB_6 model to other rare-earth hexaborides and dodecaborides

How and why could the discovered vibronic structure of SmB_6 relate to that of other rare-earth hexaborides? They all have the same cubic structures, but dramatically varying properties.[5-23] For example, EuB_6 and SmB_6 both have an anomalous peak in the specific heat, while for LaB_6 no such peak exists. *T* and *p*-sensitive magnetization, resistivity, and electronic phase transitions have been seen also in EuB_6, GdB_6, PrB_6, and YbB_6. GdB_6, and PrB_6 have easily accessible structural distortions. These observations resonate with different structural and electronic aspects of the SmB_6 model. It is likely that the types and strengths of the B-B and M-B bonds that these hexaborides can afford are the unifying factors governing their similarities and differences. For example, the radius of the rare-earth atom influences the lattice size, and thus the B-B separation in the dimers and the strength of the $\sigma(p_z)$-bond. The number of available f-electrons in the rare-earths may play a role in strengthening or weakening the interaction with the boron (Ref 25, main text). Both effects would impact the accessibility of the possible bonded M-B/B-B states, the energy splitting between them, and the vibronic couplings, which could be the building blocks of a unifying model for the entire hexaboride series. Similar phenomenology has also recently been reported in YbB_{12}.[24] Here, too, a similar kind of mixed valency is likely in play,[25] but with a more complex fundamental unit than a B_2 dimer, beyond the reach of the present computational tools.

Raman spectroscopy.

Phonon line shapes.

In the absence of electron-phonon coupling and disorder a line shape of a phonon is typically described by a Lorentz function, while disorder in a system leads to a change of phonon line shapes to Gaussian function.[26] The width (typically defined as width at half

maximum) of an observed phonon with a frequency ω is determined by disorder, if it is present, and a thermal population of the phonon levels with $\omega_{ph}=\omega/2$ through scattering on which the non-radiational decay of the excited phonons states occurs.[27] It follows the general formula $\Gamma(\mathrm{T},\omega) = \Gamma_D + A\left(2n_B\left(\frac{\omega}{2}\right)+1\right)$, where Γ_D is a temperature independent term defined by disorder.

The coupling of the A_{1g} phonon of SmB_6 to a continuum of interband electronic excitations results in a so-called Fano line shape of the phonon. This asymmetric line shape is a result of an interaction of a phonon mode with a background continuum, and can be described by an empirical formula $F(\omega,\omega_F,\Gamma_F,\mathrm{q}) = \frac{1}{\Gamma_F q^2}\frac{[q+\alpha(\omega)]^2}{1+\alpha(\omega)^2}$, where $\alpha(\omega) = \frac{\omega-\omega_F}{\Gamma_F}$, q is an empirical coupling parameter between the phonon and the electronic background.[28,29]

Intensities of the features around 20meV

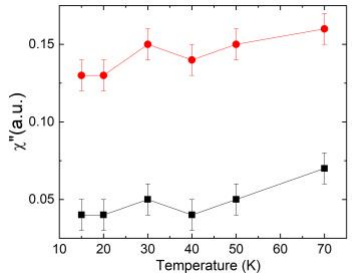

Figure S3. Intensities of the features which appear due to electron-phonon coupling as a result of valence fluctuations in the region of 20 meV. Intensity of the narrow phonon feature is shown in red, intensity of the exciton-polaron feature is shown in black.

References:

[1] Werner HJ, Knowles PJ, Knizia G, Manby FR, Schütz M (2012) Molpro: a general-purpose quantum chemistry program package. *Wiley Interdiscip. Rev. Comput. Mol. Sci.* 2:242-253.

[2] Lu Q, Peterson KA (2016) Correlation consistent basis sets for lanthanides: The atoms La–Lu. *J. Chem. Phys.* 145:054111.

[3] Dunning TH, Jr. (1989) Gaussian basis sets for use in correlated molecular calculations. I. The atoms boron through neon and hydrogen. *J. Chem. Phys.* 90:1007-1023.

[4] Liu W, Peng D (2006) Infinite-order quasirelativistic density functional method based on the exact matrix quasirelativistic theory. *J. Chem. Phys* 125:044102.

[5] Sakai T, Oomi G, Uwatoko Y, Kunii S (2007) Effect of pressure on the metamagnetic transition of DyB_6 single crystal. *J. Magnetism Magnet. Mater.* 310:1732-1734.

[6] Dorenbos P (2003) Systematic behavior in trivalent lanthanide charge transfer energies. *J. Phys.: Condens. Matter* 15:8417-8434.

[7] Batnova M, Batko I, Bauer E, Khan RT, Filipov VB, Konovalova ES (2010) Effect of pressure on the electric transport properties of carbon-doped EuB_6. *Solid State Comm.* 150:652-654.

[8] Goodrich RG, Harrison N, Vuillemin JJ, Teklu A, Hall DW, Fisk Z, Young D, Sarrao J (1998) Fermi surface of ferromagnetic EuB_6. *Phys. Rev. B* 58:148096-14902.
[9] Weill G, Smirnov IA, Gurin VN (1979) Electrical Transport Properties of EuB_6 under Pressure. New Experimental Data. *Phys. Stat. Sol. (a)* 53:K119-K123.
[10] Fujita T, Suzuki M, Isikawa Y (1980) Specific Heat of EuB_6. *Solid State. Comm* 33:947-950.
[11] Hidaka H, Ikeda Y, Kawasaki I, Yanagisawa T, Amitsuka H (2009) Specific heat of $EuIn_2P_2$ at high magnetic fields. *Physica B* 404:3005-3007.
[12] Nozaki H, Tanaka T, Ishizawa Y (1980) Magnetic behavior and structure change of GdB_6 single crystals at low temperatures. *J. Phys. C: Soid State Phys.* 13:2751-2763.
[13] Kunii S, Takeuchi K, Oguro I, Sugiyama K, Ohya A, Yamada M, Koyoshi Y, Date M, Kasuya T (1985) Electronic and magnetic properties of GdB_6. *J. Magnetism Mgn. Mater* 52:275-278.
[14] Grechnev GE, Logosha AV, Panfilov AS, Shitsevalova NY (2012) Pressure effects on magnetic properties and electronic structure of EuB_6 and GdB_6. *J. Alloys Comp*., 511:5-8.
[15] McCarthy CM, Tompson CW (1980) Magnetic structure of NdB_6. *J. Phys. Chem. Solids* 41:1319-1321.
[16] Goodrich RG, Harrison N, Fisk Z (2006) Fermi Surface Changes across the Neel Phase Boundary of NdB_6. *Phys. Rev. Lett.* 97:14604.
[17] Lazukov VN, Alekseev PA, Shitsevalova NY, Philippov VB (2016) Thermal Evolution of Magnetic-Excitation Spectrum of PrB_6. *Fizika Metallov I Metallovedenie* 117:478-484.
[18] Kuromaru T, Kusunose H, Kuranoto Y (2002) Multipolar ordering in PrB_6. *J. Phys. Soc. Jpn.* 71:130-132.
[19] Sera M, Kim M-S, Tou H, Kunii S (2004) Crystal Structure and Magnetic Anisotropy in the Magnetic Ordered Phases of PrB_6. *J. Phys. Soc. Jpn*. 73:3422-3428.
[20] Deng X, Haule K, Kotliar G (2013) Plutonium Hexaboride is a Correlated Topological Insulator. *Phys. Rev. Lett.* 111:176404.
[21] Xu N, Biswas PK, Dil JH, Dhaka RS, et al (2014) Direct observation of the spin texture in SmB_6 as evidence of the topological Kondo insulator. *Nat. Comm*. 5:4566.
[22] Zhou Y, Kim D-J, Rosa PFS, Wu Q, Guo J, et al (2015) Pressure-induced quantum phase transitions in a YbB_6 single crystal. *Phys. Rev. B* 92:241118(R).
[23] Kang C-J, Denlinger JD, Allen JW, Min CH, Reinert F, Kang BY, Cho BK, Kang J-S, Shim JH, Min BI (2016) Electronic Structure of YbB_6: Is it a Topological Insulator of Not? *Phys. Rev. Lett.* 116:116401.
[24] (a) Xiang Z, Kasahara Y, Asaba T, Lawson B, Tinsman C, Lu Chen L, Sugimoto K, Kawaguchi S, Sato Y, Li G, Yao S, Chen YL, Iga F, Singleton J, Matsuda Y, Li L (2018) Quantum oscillations of electrical resistivity in an insulator. *Science* 362:65-69
(b) P. A. Alexeyev (2015) High borides: determining the features and details of lattice dynamics from neutron spectroscopy. *Physics-Uspekhi*, 58:330-344.
[25] Mizokawa T (2015) Evidence for Γ_8 Ground-State Symmetry of Cubic YbB_{12} Probed by Linear Dichroism in Core-Level Photoemission. *J. Phys. Soc. Jpn.* 84:073705.
[26] Hollas MJ (1996) *Modern Spectroscopy* (Wiley, ed. 3) pp. 30–34
[27] Kim Y, Chen X, Wang Z, Shi J, Miotkowski I, Chen YP, Sharma PA, Lima Sharma AL, Hekmaty MA, Jiang Z, Smirnov D (2012) Temperature dependence of Raman-active optical phonons in Bi_2Se_3 and Sb_2Te_3. *Applied Physics Letters* 100:071907.

[28] Zhang WL, Li H, Xia D, Liu HW, Shi YG, Luo JL, Hu J, Richard P, Ding H (2015) Observation of a Raman-active phonon with Fano line shape in the quasi-one-dimensional superconductor $K_2Cr_3As_3$. *Physical Review B* 92:060502.
[29] Fano U. (1961) Effects of configuration interaction on intensities and phase shifts. *Physical Review* 124:1866.